PROCEEDINGS OF SCIENCE

Heavy Flavor Spectroscopy and Exotica with ATLAS

Paolo Iengo* **on behalf of the ATLAS Collaboration**
CERN
E-mail: paolo.iengo@cern.ch

The paper presents a review of recent heavy-flavour spectroscopy studies performed with the ATLAS experiment using the data collected during the LHC Run 1. It includes the study of the $B_c^+ \to J/\psi D_s^+$ and $B_c^+ \to J/\psi D_s^{*+}$ decays, the first observation of an excited $B_c^{\pm}$ meson state, the production measurements of $\psi(2S)$ and X(3872) decaying to $J/\psi\pi^+\pi^-$ and the search for X_b and other hidden-beauty states in $\pi^+\pi^-\Upsilon(1S)$ channel.

Forth Annual Large Hadrn Collider Physics
13-8 June, 2016
Lund, Sweden

*Speaker.

PoS(LHCP2016)068

1. Introduction

The LHC provides a good environment for studies of heavy-flavour spectroscopy. Both measurements of properties of the known states and searches for new ones are possible. In this paper, four results obtained by the ATLAS experiment [1] with the Run1 data are presented: the study of the $B_c^+ \to J/\psi D_s^+$ and $B_c^+ \to J/\psi D_s^{*+}$ decays [2], the first observation of an excited $B_c^{\pm}$ meson state [3], the production measurements of $\psi(2S)$ and X(3872) decaying to $J/\psi\pi^+\pi^-$ [4] and the search for X_b and other hidden-beauty states in $\pi^+\pi^-\Upsilon(1S)$ channel [5].

2. Branching fractions of $B_c^+ \to J/\psi D_s^+$ and $B_c^+ \to J/\psi D_s^{*+}$ and transverse polarization fraction in the latter decay

The B_c^+ meson[1] is the only known weakly decaying particle consisting of two heavy quarks. The presence of two heavy quarks, each of which can decay weakly, affects theoretical calculations of the decay properties of the B_c^+ meson. The measurements of B_c^+ properties is thus relevant to test theoretical predictions. In particular the decay $B_c^+ \to J/\psi D_s^{*+}$ is a transition of a pseudoscalar meson into a pair of vector states and is thus described by the three helicity amplitudes, A_{00}, A_{++} and A_{--}, where the subscripts correspond to the helicities of J/ψ and D_s^{*+}. The contribution of the A_{++} and A_{--} amplitudes, referred to as the $A_{\pm\pm}$ component, corresponds to the J/ψ and D_s^{*+} transverse polarisation.

The decays $B_c^+ \to J/\psi D_s^+$ and $B_c^+ \to J/\psi D_s^{*+}$ are studied with the ATLAS detector using a dataset corresponding to integrated luminosities of 4.9 fb[1] and 20.6 fb[1] of pp collisions collected at centre-of-mass energies $\sqrt{s}$ = 7 TeV and 8 TeV, respectively. Signal candidates are identified through $J/\psi \to \mu^+\mu^-$ and $D^{(*)+} \to \phi\pi^+(\gamma\pi^0)$ decays. Figure 1 left shows the mass distribution for the selected $J/\psi D_s^+$ candidates where the J/ψ and D_s^+ mass distributions are fitted with a sum of an exponential function describing the background and a modified Gaussian function [6] [7] describing the corresponding signal peak. Figure 1 right shows the distribution of the variable $|\cos\theta'(\mu^+)|$, where the helicity angle $\theta'(\mu^+)$ is the angle between the μ^+ and D_s^+ candidate momenta in the rest frame of the muon pair from J/ψ decay, for a subset of the candidates in a mass range 5950 MeV < $m(J/\psi D_s^+)$ < 6250 MeV corresponding to the observed signal of $B_c^+ \to J/\psi D_s^{*+}$ decay.

With a two-dimensional likelihood fit involving the B_c^+ reconstructed invariant mass and $|\cos\theta'(\mu^+)|$, the yields of $B_c^+ \to J/\psi D_s^+$ and $B_c^+ \to J/\psi D_s^{*+}$ and the transverse polarisation fraction in $B_c^+ \to J/\psi D_s^{*+}$ decay are measured. The fraction of transverse polarisation, $\Gamma_{\pm\pm}/\Gamma = \Gamma_{\pm\pm}(B_c^+ \to J/\psi D_s^{*+})/\Gamma(B_c^+ \to J/\psi D_s^{*+})$, is also measured[2]. The derived ratio of the branching fractions of the two modes is $\mathscr{B}_{B_c^+ \to J/\psi D_s^{*+}}/\mathscr{B}_{B_c^+ \to J/\psi D_s^+} = 2.8^{+1.2}_{-0.8} \pm 0.3$ where the first error is statistical and the second is systematic. A sample of $B_c^+ \to J/\psi\pi^+$ decays is used to derive the ratios of branching fractions $\mathscr{B}_{B_c^+ \to J/\psi D_s^+}/\mathscr{B}_{B_c^+ \to J/\psi\pi^+} = 3.8 \pm 1.1 \pm 0.4 \pm 0.2$ and $\mathscr{B}_{B_c^+ \to J/\psi D_s^{*+}}/\mathscr{B}_{B_c^+ \to J/\psi\pi^+} = 10.4 \pm 3.1 \pm 1.5 \pm 0.6$ where the third error corresponds to the uncer-

[1] Charge conjugate states are implied throughout the paper unless otherwise stated.

[2] From a naive prediction by spin counting, one would expect this fraction to be 2/3, while calculations [8] and [9] predict values of 0.41-0.48.

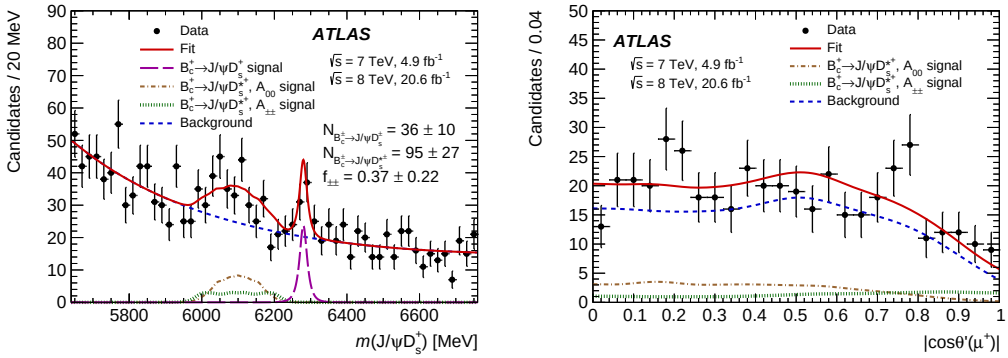

Figure 1: Left: The mass distribution for the selected $J/\psi D_s^+$ candidates. The red solid line represents the projection of the fit to the model described in the text. The contribution of the $B_c^+ \to J/\psi D_s^+$ decay is shown with the magenta long-dashed line; the brown dash-dot and green dotted lines show the $B_c^+ \to J/\psi D_s^{*+}$, A_{00} and $A_{\pm\pm}$ component contributions, respectively; the blue dashed line shows the background model. The uncertainties of the listed fit result values are statistical only. Right: The projection of the likelihood fit on the variable $|\cos\theta'(\mu^+)|$, where the helicity angle $\theta'(\mu^+)$ is the angle between the μ^+ and D_s^+ candidate momenta in the rest frame of the muon pair from J/ψ decay, for a subset of the candidates in a mass range 5950 MeV $< m(J/\psi D_s^+) <$ 6250 MeV corresponding to the observed signal of $B_c^+ \to J/\psi D_s^{*+}$ decay. The red solid line represents the full fit projection. The brown dash-dot and green dotted lines show the $B_c^+ \to J/\psi D_s^{*+}$ A_{00} and $A_{\pm\pm}$ component contributions, respectively; the blue dashed line shows the background model.

tainty of the branching fraction of $D_s^+ \to \phi(K^+K^-)\pi^+$ decay. Finally, the transverse polarisation fraction is determined to be $\Gamma_{\pm\pm}/\Gamma = 0.38 \pm 0.23 \pm 0.07$.

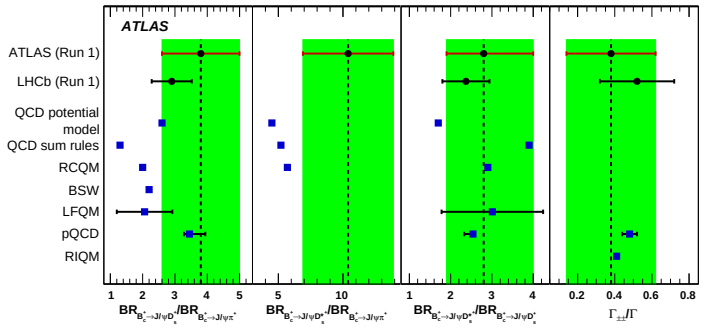

Figure 2: Comparison of the results of this measurement with those of LHCb [10] and theoretical predictions based on a QCD relativistic potential model [11], QCD sum rules [12], relativistic constituent quark model (RCQM) [13], BSW relativistic quark model (with fixed average transverse quark momentum ω = 0.40 GeV) [14], light-front quark model (LFQM) [15], perturbative QCD (pQCD) [16], and relativistic independent quark model (RIQM) [17]. The uncertainties of the theoretical predictions are shown if they are explicitly quoted in the corresponding papers. Statistical and systematic uncertainties added in quadrature are quoted for the results of ATLAS and LHCb.

Figure 2 shows in a grafical form the comparison between the ATLAS measurements with those of LHCb and several theoretical predictions. The polarisation is found to be well described by the available theoretical approaches. The measured ratios of the branching fraction are generally described by perturbative QCD, sum rules, and relativistic quark models. There is an indication of

underestimation of the decay rates for the $B_c^+ \to J/\psi D_s^+$ decays by some models, although the discrepancies do not exceed two standard deviations when taking into account only the experimental uncertainty. The measurement results agree with those published by the LHCb experiment.

3. Observation of an excited B_c^+ meson state

Spectrum and properties of excited B_c^+ mesons are predicted by non-relativistic potential models, perturbative QCD, and lattice calculations (see reference 5 in Ref. [3]). Thus, observations and measurements of these states can provide a mean to test those predictions and ultimately to extract information on the strong interaction potential. A good candidate for experimental search is a pseudo-scalar state of $B_c^+(2S)$ decaying into a ground state (2S) and a pair of pions. The ATLAS analysis uses the full sample of pp collisions data collected at $\sqrt{s}$ =7 TeV and 8 TeV corresponding to integrated luminosities of 4.9 fb^{-1} and 19.2 fb^{-1}, respectively. The ground state B_c^+ is reconstructed in $B_c^+ \to J/\psi(\mu^+\mu^-)\pi^+$ decay mode. The candidates are built by combining two tracks identified as muons with one additional track with assigned pion mass and fitting them to a common vertex. Requirements on the tracks, the candidate kinematics and the vertex fit quality are applied. The pion is also required to have high significance of the transverse impact parameter with respect to the primary vertex, which allows to substantially reduce the combinatorial backgrounds. Figure 3 shows the mass distribution of the reconstructed candidates in 7 TeV and 8 TeV data. They are fitted with a sum of a Gaussian shape to describe the signal peak and an exponential function for the background.

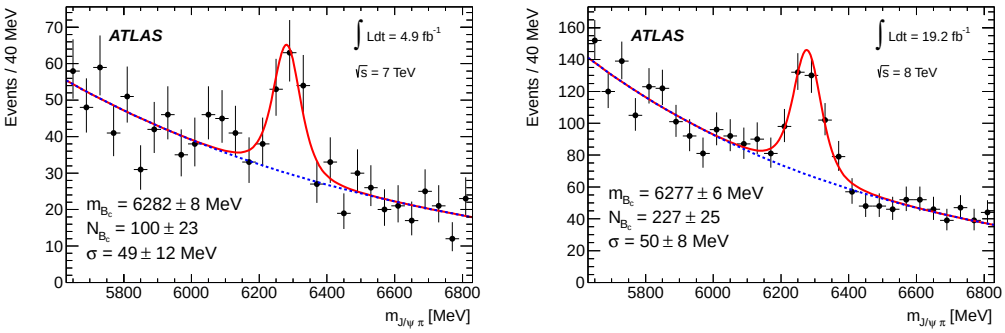

Figure 3: Invariant mass distributions of the reconstructed $B_c^+ \to J/\psi\pi^+$ candidates in 7 TeV (left) and 8 TeV (right) data. The data are represented by the points with error bars (statistical only). The solid line is the projection of the results of the unbinned maximum likelihood fit to all candidates in the mass range 5620-6820 MeV. The dashed line is the projection of the background component of the same fit.

The $B_c^+(2S) \to B_c^+\pi^+\pi^-$ candidates are formed by combining a B_c^+ candidate with two oppositely charged hadronic tracks from the primary vertex. A cascade fit is performed, requiring the B_c^+ combined momentum to point back to the primary vertex. If more than one $B_c^+(2S)$ candidate is found in an event, the one with the best cascade fit is selected. The $B_c^+(2S)$ signal is searched for in the distribution of $Q = m(B_c^+\pi^+\pi^-) - m(B_c^+) - 2m(\pi)$, in order to reduce the effects of the ground state B_c^+ mass resolution. Figure 4 shows the distributions of this variable for the $B_c^+(2S)$ candidates selected in 7 TeV and 8 TeV data. Clear peaking structure are seen in both datasets. To

extract the signal yields, the Q distributions are fitted with a sum of a Gaussian function and a third order polynomial function to describe the observed peak and the background, respectively. The Q distributions for wrong charge combinations where the two pions from the primary vertex have the same sign are used to control the background behaviour and are also shown in Figure 4. The peak positions, widths, and the yields obtained from the fit are quoted on the plots with only statistical uncertainty.

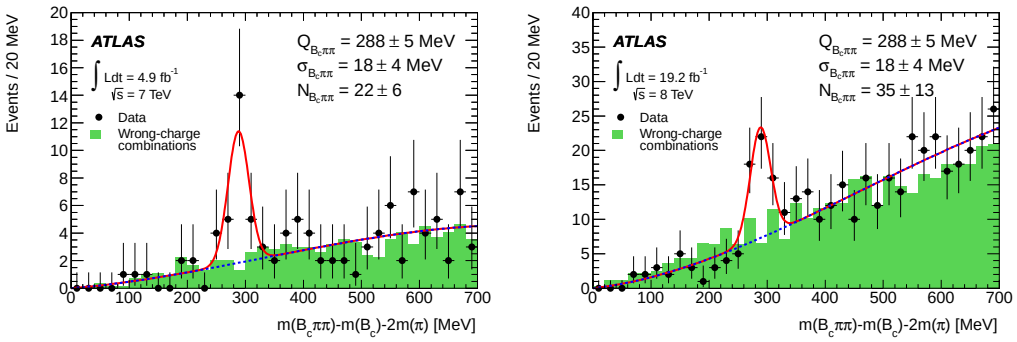

Figure 4: The $Q = m(B_c^+\pi^+\pi^-) - m(B_c^+) - 2m(\pi)$ distribution for the right-charge combinations (points with error bars) and for the same (wrong) pion charge combinations (shaded histogram) in 7 TeV (left) and 8 TeV (right) data. The wrong-charge combinations are normalized to the same yield as the right-charge background. The solid line is the projection of the results of the unbinned maximum likelihood fit to all candidates in the range 0-700 MeV. The dashed line is the projection of the background component of the same fit.

The weighted average value of Q in the two datasets is $Q = 288.3 \pm 3.5 \pm 4.1$ MeV where the first error is statistical and the secod systematics, corresponding to the mass of the new state of $6842 \pm 4(\text{stat.}) \pm 5(\text{syst.})$ MeV. The statistical uncertainty is dominated by the uncertainty of the ground state B_c^+ mass and the Q distribution fitting procedure.

The statistical significance of the signal is evaluated with toy Monte Carlo studies and accounts for the so called look-elsewhere effect [18]. It is found to be 3.7σ and 4.5σ in 7 TeV and 8 TeV data, respectively, and the combined significance is 5.2σ. Thus, a new state is observed in the $B_c^+\pi^+\pi^-$ channel with the ATLAS data. Its measured mass is consistent with the theoretical predictions for the $B_c^+(2S)$ excited state.

4. Production measurements of $\psi(2S)$ and X(3872) $\to J/\psi\pi^+\pi^-$

A particularly interesting aspect of the hidden-charm state X (3872) is the closeness of its mass 3871.69 4±0.17 MeV [19] to the $D^0\bar{D}^{*0}$ threshold, such that it was hypothesised to be a $D^0\bar{D}^{*0}$ molecule with a very small binding energy [20]. A later interpretation of X(3872) as a mixed $\chi_{c1}(2P) - D^0\bar{D}^{*0}$ state, where the X(3872) is produced predominantly through its $\chi_{c1}(2P)$ component, was used with the NLO NRQCD model [21].

ATLAS has previously observed the X(3872) state during the cross-section measurement of prompt and non-prompt $\psi(2S)$ meson production in the $J/\psi\pi^+\pi^-$ decay channel with 2011 data at a centre-of-mass energy $\sqrt{s}$ = 7 TeV [22]. In the analysis reported here, a measurement of the differential cross sections for the production of $\psi(2S)$ and X(3872) states in the decay channel

$J/\psi\pi^+\pi^-$ is performed, using 11.4 fb^{-1} of proton-proton collision data collected by the ATLAS experiment at the LHC at $\sqrt{s}$ = 8 TeV. The $J/\psi\pi^+\pi^-$ final state allows for an improved invariant mass resolution through the use of a constrained fit, and provides a straightforward way of comparing the production characteristics of $\psi(2S)$ and X(3872) states, which are fairly close in mass. $\psi(2S)$ and X(3872) candidates are recontructed with a 4-track vertex fit of a di-muon pair (from the J/ψ candidates) and two oppositely charged non-muon tracks. Figure 5 left shows the invariant mass distribution of the selected $J/\psi\pi^+\pi^-$ candidates collected over the full p_T range 10-70 GeV and the rapidity range |y|<0.75 after selection cuts. The distribution is fitted using a double Gaussian for the $\psi(2S)$ and X(3872) peaks and a fourth-order polynomial for the background.

The prompt and non-prompt contributions for $\psi(2S)$ and X(3872) are separated, based on the analysis of the displacement of the production vertex, looking to the pseudo-proper time $\tau = L_{xy} m/cp_T$ where m is the invariant mass and L_{xy} is the transverse decay lenght of the $J/\psi\pi^+\pi^-$ candidate defined as $L_{xy} = \vec{L}\cdot\vec{p}_T/p_T$. Figure 5 right shows the measured effective pseudo-proper lifetimes for non-prompt X(3872) and $\psi(2S)$. Non-prompt production fractions for $\psi(2S)$ and X(3872) are also measured, as well as the X(3872)/$\psi(2S)$ production ratios, separately for prompt and non-prompt components (see [4]).

Figure 6 shows the cross section times branching fractions of the X(3872) in p_T bins from 10 to 70 GeV for prompt (left) and non-prompt (right) components. Good agreement is found with theoretical predictions within the NLO NRQCD model, which considers X(3872) to be a mixture of $\chi_{c1}(2P) - D^0\bar{D}^{*0}$ molecular state, with the production being dominated by the $\chi_{c1}(2P)$ component.

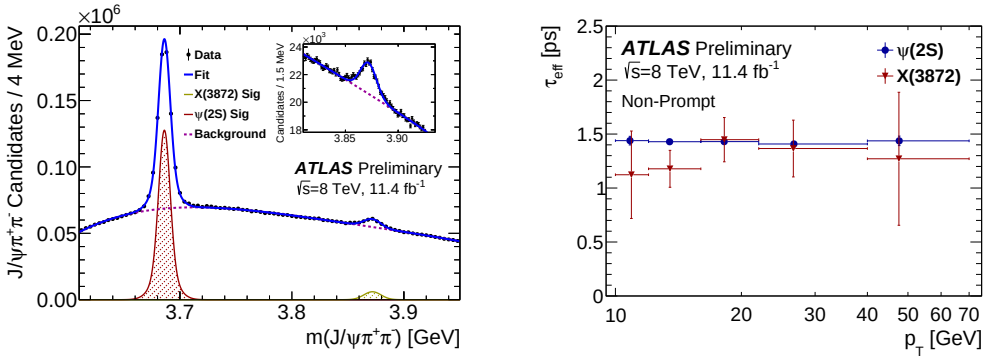

Figure 5: Left: Invariant mass of the selected $J/\psi\pi^+\pi^-$ candidates collected over the full p_T range 10-70 GeV and the rapidity range |y|<0.75 after selection cuts. The curve shows the results of the fit using double Gaussians for the and $\psi(2S)$ and X(3872) peaks and a fourth-order polynomial for the background. The X(3872) mass range is highlighted in the inset. Right: Measured effective pseudo-proper lifetimes for non-prompt X(3872) and $\psi(2S)$.

5. Search for X_b and other hidden-beauty states in $\pi^+\pi^-\Upsilon(1S)$ channel

The X(3872) is the best-studied of the new hidden-charm state seen in the last decade. Its mass, narrow width, quantum numbers and decay properties measured in several experiments make it unlikely to be a conventional quarkonium state, and various theoretical models are proposed in the literature to describe its structure. Heavy-quark symmetry suggests the existence of a hidden-

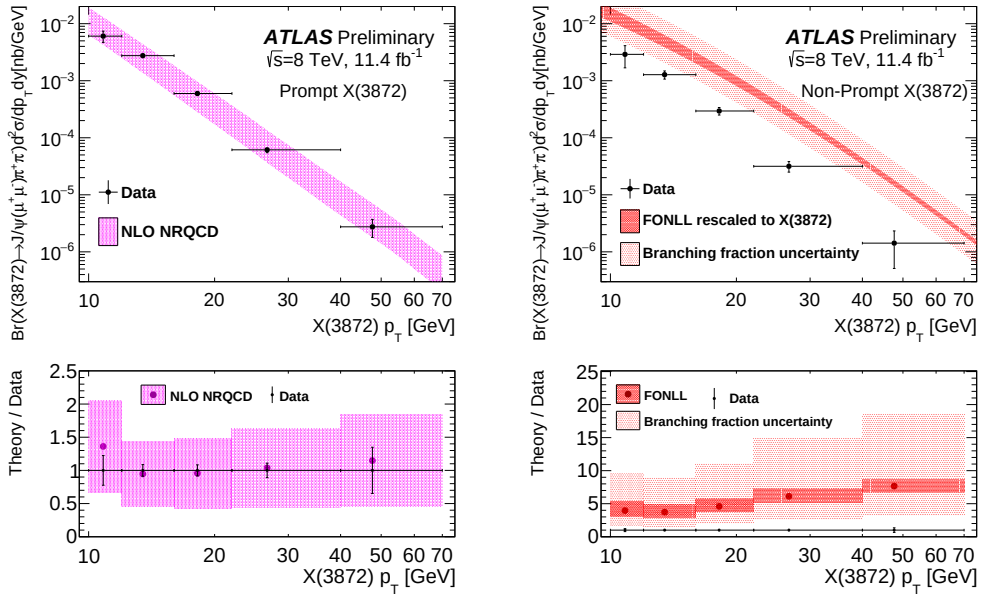

Figure 6: Measured cross section times branching fractions as a function of p_T for (left) prompt X(3872) compared to NLO NRQCD predictions with the X(3872) modelled as a mixture of $\chi_{c1}(2P) - D^0\bar{D}^{*0}$ molecular state [21], and (right) non-prompt X(3872) compared to the FONLL [23] model prediction, recalculated using the branching fraction estimate from [24].

beauty partner referred to as X_b which should be produced in pp collisions. The ATLAS experiment has performed a search for this particle in $\pi^+\pi^-\Upsilon(1S)$ channel with the pp collision data collected at $\sqrt{s} = 8$ TeV in 2012. The $\Upsilon(1S)$ candidates are built from two muon tracks. The candidates with the invariant mass within ± 350 MeV window around the nominal $\Upsilon(1S)$ mass are retained. They are combined with two tracks with assigned pion mass and a 4-prong vertex fit is performed. The muon pair mass is constrained to the world average for the $\Upsilon(1S)$ to improve the $X_b \to \pi^+\pi^-\Upsilon(1S)$ mass resolution. The whole data sample is separated into 8 kinematic bins with different signal sensitivity. First, based on the rapidity y of the X_b candidate, the barrel ($|y| < 1.2$) and endcap ($1.2 < |y| < 2.4$) regions having different invariant mass resolution are separated. Each of these sub-samples is then split into four bins with different signal-to-background ratio. This splitting is defined using the candidate transverse momentum p_T and $\cos\theta^*$, where θ^* is the angle between $\pi^+\pi^-$ combined momentum in the parent momentum rest frame and the parent momentum in the laboratory frame. Expected fractions of the signal in each bin are defined by splitting functions derived from the simulation. Figure 7 shows the distribution of the $\pi^+\pi^-\Upsilon(1S)$ invariant mass. Only peaks at the masses corresponding to $\Upsilon(2S)$ and $\Upsilon(3S)$ signals are seen. These signals are used to validate correctness of the splitting functions and check agreement of the yields between data and simulation.

To search for the X_b signal, a hypothesis test for the presence of a peak is performed every 10 MeV in the $\pi^+\pi^-\Upsilon(1S)$ mass range from 10 GeV to 11 GeV. At each mass, a simultaneous fit to all analysis bins is performed. A double Gaussian function is used in the fits for the expected signal shape thus assuming its width to be negligible with respect to the detector resolution. Other

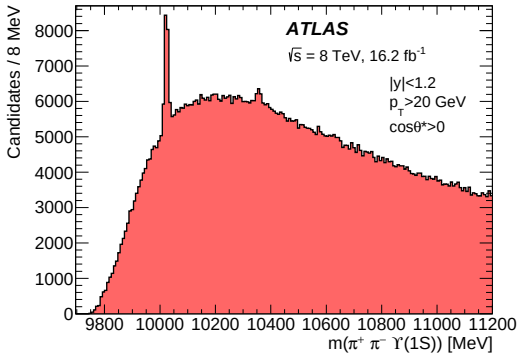

Figure 7: The $\pi^+\pi^-\Upsilon(1S)$ invariant mass distribution in the kinematic bin most sensitive to an X_b signal: $|y| < 1.2$, $p_T > 20$ GeV, and $\cos\theta^* > 0$. The only apparent peaks are at the masses of the $\Upsilon(2S)$ (10023 MeV) and $\Upsilon(3S)$ (10355 MeV).

constraints used in the fit procedure assume the resolution dependence on y and p_T being the same as that for $\Upsilon(2S)$ and $\Upsilon(3S)$ states and the phase-space distribution of the di-pion invariant mass. An upper limit on the value of $R = (\sigma\mathscr{B})/(\sigma\mathscr{B})_{2S}$ is set using the CL_S method [25]. The $R = (\sigma\mathscr{B})$ is a product of the hypothetical state production cross-section and the branching fraction of its decay to $\pi^+\pi^-\Upsilon(1S)$ while $(\sigma\mathscr{B})_{2S}$ is the same quantity for the $\Upsilon(2S)$. Various systematic uncertainties were studied and included in the fit likelihood as nuisance parameters to be accounted in the limit setting. Figure 8 shows the 95% CL_S limit on R as a function of the X_b mass. The mass regions close to $\Upsilon(2S)$ and $\Upsilon(3S)$ resonances are excluded from the analysis due to poor sensitivity.

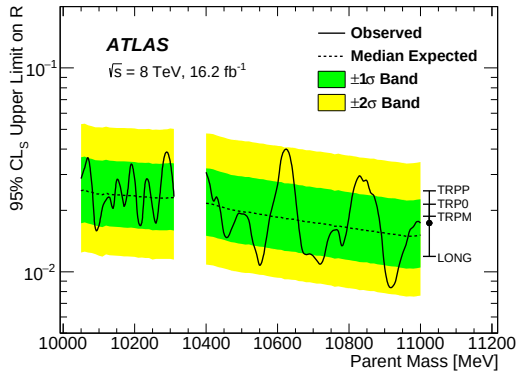

Figure 8: Observed 95% CL_S upper limits (solid line) on the relative production rate $R = (\sigma\mathscr{B})/(\sigma\mathscr{B})_{2S}$ of a hypothetical X_b parent state decaying isotropically to $\pi^+\pi^-\Upsilon(1S)$, as a function of mass. The median expectation (dashed) and the corresponding $\pm1\sigma$ and $\pm2\sigma$ bands (green and yellow respectively) are also shown. The bar on the right shows typical shifts under alternative X_b spin-alignment scenarios, relative to the isotropic ("FLAT") case shown with the solid point.

The procedure assumes unpolarised production of the X_b state. However the X_b spin-alignment is unknown and can have a strong impact on the upper limit calculation. Rather than including this as a systematic uncertainty, upper limits are recalculated under longitudinal ("LONG") and three transverse ("TRPP", "TRP0", "TRPM") spin-alignment scenarios. Shifts in the upper limits (either up or down) depend only weakly on mass. Thus in Figure 8 the effect of each hypothesis is repre-

sented by a single number, chosen as a difference in the median expected CL_S from the unpolarised ("FLAT") case. No evidence of X_b signal is found. A 95% CL_S upper limit on $(\sigma\mathscr{B})/(\sigma\mathscr{B})_{2S}$ is set at level of 0.8-4.0% depending on mass. The analogous ratio for the X(3872) state is 6.56%: a value this large is excluded for all X_b masses considered.

Within the same analysis framework, searches for the $\Upsilon(1^3D_J)$ triplet as well as for wide resonances $\Upsilon(10860)$ and $\Upsilon(11020)$ states were performed. For these signals, the fit model was modified accordingly. None of these searches resulted in a signal evidence. For the triplet, an upper limit on the ratio of cross-sections $\sigma(\Upsilon(1^3D_J))/\sigma(\Upsilon(2S)) < 0.55$ is set.

6. Concusions

ATLAS performed a rich reasearch program in the heavy flavor spettroscopy and in searching for new exotic states. Four studies based on data collected during LHC Run 1 have been presented here: the study of the $B_c^+ \to J/\psi D_s^+$ and $B_c^+ \to J/\psi D_s^{*+}$ decays, the first observation of an excited $B_c^{\pm}$ meson state, the production measurements of $\psi(2S)$ and X(3872) decaying to $J/\psi\pi^+\pi^-$ and the search for X_b and other hidden-beauty states in $\pi^+\pi^-\Upsilon(1S)$.

7. Aknowledgements

Author would like to aknowledge the organizers of the LHCP2016 Conference in Lund.

References

[1] ATLAS Collaboration, The ATLAS Experiment at the CERN Large Hadron Collider, JINST 3 (2008) S08003

[2] Eur. Phys. J. C, 76(1), 1 (2016)

[3] Phys. Rev. Lett. 113 (2014) 212004

[4] ATLAS-CONF-2016-028

[5] Phys. Lett. B740 (2015) 199-217

[6] Eur. Phys. J. C 44 (2005) 13-25

[7] Nucl. Phys. B 864 (2012) 341-381

[8] Phys. Rev. D 90 (2014) 114030

[9] Phys. Rev. D 88 (2013) 094014

[10] Phys. Rev. D 87 (2013) 112012

[11] Phys. Rev. D 61 (2000) 034012

[12] arXiv:hep-ph/0211021 [hep-ph]

[13] Phys. Rev. D 73 (2006) 054024

[14] Phys. Rev. D 79 (2009) 034004,

[15] Phys. Rev. D 89 (2014) 017501

[16] Phys. Rev. D 90 (2014) 114030

[17] Phys. Rev. D 88 (2013) 094014

[18] Eur. Phys. J. C 70 (2010) 525-530

[19] Review of Particle Physics, Chin. Phys. C38 (2014) 090001

[20] Phys. Rev. D91 (2015) 011102

[21] arXiv: 1304.6710 [hep-ph]

[22] JHEP 1409 (2014) 079

[23] JHEP 10 (2012) 137

[24] Phys. Rev. D81 (2010) 114018

[25] Eur. Phys. J. C 71 (2011) 1554